as a general guide to amphiphile monolayer assembly. In addition to improving our basic knowledge of molecular self-assembly, these results may be useful in guiding efforts to grow more highly ordered films and self-assembled supramolecular architectures.

REFERENCES AND NOTES

1. L. Haussling, W. Knoll, H. Ringsdorf, F.-J. Schmitt, J. Yang, *Makromol. Chem. Macromol. Symp.* **46**, 145 (1991).
2. P. A. DiMilla *et al.*, *J. Am. Chem. Soc.* **116**, 2225 (1994).
3. O. Chailapakul, L. Sun, C. Xu, R. M. Crooks, *ibid.* **115**, 12459 (1993).
4. L. C. F. Blackman and M. J. S. Dewar, *J. Chem. Soc.* **1957**, 162 (1957).
5. L. H. Dubois and R. G. Nuzzo, *Annu. Rev. Phys. Chem.* **43**, 437 (1992).
6. N. Camillone, C. E. D. Chidsey, G.-y. Liu, G. Scoles, *J. Chem. Phys.* **98**, 3503 (1993); G. E. Poirier and M. J. Tarlov, *Langmuir* **10**, 2853 (1994).
7. C. D. Bain and G. M. Whitesides, *J. Am. Chem. Soc.* **111**, 7164 (1989).
8. R. C. Thomas, L. Sun, R. M. Crooks, A. J. Ricco, *Langmuir* **7**, 620 (1991).
9. M. Buck, M. Grunze, F. Eisert, J. Fischer, F. Trager, *J. Vac. Sci. Technol. A* **10**, 926 (1992).
10. G. Hahner, C. Woll, M. Buck, M. Grunze, *Langmuir* **9**, 1955 (1993).
11. D. S. Karpovich and G. J. Blanchard, *ibid.* **10**, 3315 (1994).
12. Our measurements were performed in a multichamber ultrahigh-vacuum (UHV) surface-analysis system that has a base pressure of 3×10^{-8} Pa (2×10^{-10} torr) and is equipped with a rapid-entry load lock. Single crystals of Au(111) were cleaned by sputtering and annealing to 500° to 600°C for 10 min. After this preparation, x-ray photoelectron spectroscopy revealed a contamination-free surface and STM topographs showed the herringbone reconstruction characteristic of clean Au(111). These topographs were used to establish the sample's crystallographic orientation with respect to the STM scan direction. For gas-phase deposition, the molecules were stored in an ambient-temperature, blackened-glass vial attached to the UHV chamber by a variable-aperture leak valve. We purified the neat alkanethiols using freeze-pump-thaw cycles and confirmed the purity using in situ quadrupole mass spectrometry. Dosing pressures were typically 1×10^{-5} Pa (1×10^{-7} torr). For liquid-phase deposition, 4.5 μM solutions of C_nX in ethanol were prepared, and the coverage was controlled by variation of the incubation time. We prepared the STM tips from single-crystal tungsten wire using a dc etch. All STM imaging was done at room temperature in constant-current mode. The tunneling-current set point was fixed between 5 and 100 pA, and the bias voltage was set between ±(200 to 400) mV.
13. A. R. Sandy, S. G. J. Mochrie, D. M. Zehner, K. G. Huang, D. Gibbs, *Phys. Rev. B* **43**, 4667 (1991).
14. C. Woll, S. Chiang, R. J. Wilson, P. H. Lippel, *ibid.* **39**, 7988 (1989).
15. D. D. Chambliss, R. J. Wilson, S. Chiang, *J. Vac. Sci. Technol. B* **9**, 933 (1991).
16. M. Zinke-Allmang, L. C. Feldman, M. H. Grabow, *Surf. Sci. Rep.* **16**, 378 (1992).
17. J. A. Stroscio, D. T. Pierce, R. A. Dragoset, P. N. First, *J. Vac. Sci. Technol. A* **10**, 1981 (1992).
18. H. Sellers, A. Ulman, Y. Shnidman, J. E. Eilers, *J. Am. Chem. Soc.* **70**, 2447 (1993).
19. P. Fenter, A. Eberhardt, P. Eisenberger, *Science* **266**, 1216 (1994).
20. N. Camillone, T. Y. B. Leung, P. Schwartz, P. Eisenberger, G. Scoles, *Langmuir*, in press.
21. K. Edinger, A. Golzhauser, K. Demota, C. Woll, M. Grunze, *Langmuir* **9**, 4 (1993); G. E. Poirier and M. J. Tarlov, *J. Phys. Chem.* **99**, 10966 (1995).
22. G. E. Poirier, E. D. Pylant, J. M. White, *J. Chem. Phys.*, in press.
23. C. Zubragel *et al.*, *Chem. Phys. Lett.* **219**, 127 (1994); A. Karpfen, *J. Chem. Phys.* **75**, 238 (1981).
24. W. D. Harkins and E. Boyd, *J. Phys. Chem.* **45**, 20 (1941).
25. N. K. Adam, *Proc. R. Soc. London Ser. A* **101**, 516 (1922).
26. N. R. Pallas and B. A. Pethica, *Langmuir* **1**, 509 (1985).

27. We gratefully acknowledge R. W. Ashton for providing purified mercaptohexanol and A. Eberhardt, R. E. Cavicchi, P. Eisenberger, G. Scoles, and J. M. White for helpful discussions. E.D.P. gratefully acknowledges financial support from NSF under the auspices of the Summer Internship Program, grant NSF CHE 9391640.

20 December 1995; accepted 7 March 1996

Dynamic Ocean-Atmosphere Coupling: A Thermostat for the Tropics

De-Zheng Sun* and Zhengyu Liu

The ocean currents connecting the western tropical Pacific Ocean with the eastern tropical Pacific Ocean are driven by surface winds. The surface winds are in turn driven by the sea-surface temperature (SST) differences between these two regions. This dynamic coupling between the atmosphere and ocean may limit the SST in the tropical Pacific Ocean to below 305 kelvin even in the absence of cloud feedbacks.

Records of past climates and observations of the interannual fluctuations about the present climate suggest that the maximum tropical SST is somehow limited to below 305 K (*1*, *2*). Ramanathan and Collins (*3*) hypothesized that the tropical Pacific SST is mainly regulated by a negative feedback from cirrus clouds, a controversial (*4*, *5*) proposal they referred to as the "thermostat hypothesis." In this report, we propose an alternative thermostat for the SST in the tropical Pacific Ocean: the dynamic coupling between the atmosphere and ocean. The ocean currents that connect the western Pacific Ocean with the eastern Pacific Ocean are driven by surface winds. Surface winds are in turn driven by the SST differences between these two regions (*6*). This dynamic coupling plays a central role in the El Niño–Southern Oscillation phenomena (*2*, *7*), but its importance for the mean tropical climate has been less clear.

To illustrate the mechanism by which the dynamic ocean-atmosphere coupling regulates the tropical SST, we consider a three-box model for the tropical Pacific Ocean coupled with a simple atmosphere (Fig. 1). The surface Pacific Ocean over the equatorial region is represented by two boxes with temperatures T_1 and T_2. The two boxes are assumed to have the same volume. The subsurface ocean is represented by another box with temperature T_c. The ocean currents are driven by surface winds. Using T_e to represent the radiative-convective equilibrium temperature, the temperature that the surface ocean would attain in the absence of the ocean currents, and c to represent the reciprocal of the time scale for the radiative-convective processes, we can write the heat budget of the two surface boxes over time t as

$$\frac{dT_1}{dt} = c(T_e - T_1) + q(T_2 - T_1) \quad (1)$$

$$\frac{dT_2}{dt} = c(T_e - T_2) + q(T_c - T_2) \quad (2)$$

with q given by

$$q = \alpha(T_1 - T_2) \quad (3)$$

where α is a constant related to the eddy-damping time scale in the atmospheric boundary layer and in the mixed layer of the ocean. The first term on the right side of Eqs. 1 and 2 is the local heat exchange with the atmosphere, and the second term is the advection of heat by the ocean currents. In deriving Eq. 3, we have assumed that the strength of the ocean cur-

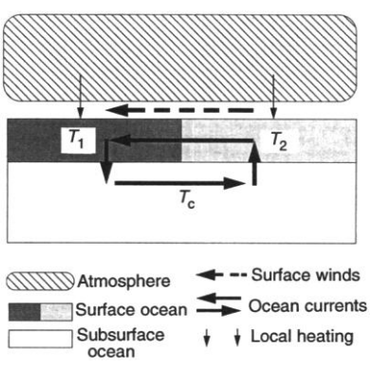

Fig. 1. A schematic diagram for the coupled model. The east-west surface current is the frictional flow driven by the east-west surface winds, and the return flow may be largely considered as the equatorial undercurrent. The east-west surface winds also drive a meridional cell that connects the equatorial subsurface ocean to the extratropical ocean (*11*).

D.-Z. Sun, National Center for Atmospheric Research, Boulder, CO 80307, USA.
Z. Liu, Department of Atmospheric and Oceanic Sciences, University of Wisconsin, Madison, WI 53706, USA.

*To whom correspondence should be addressed.

rents is proportional to the strength of the surface winds, and that the strength of the surface winds is proportional to the east-west SST gradients (6). Because the simple coupled system does not contain any physics that distinguishes the east from the west, we have also assumed $q \geq 0$. In addition, T_c is assumed to have a fixed value (8).

The behavior of the simple coupled system constituted by Eqs. 1 through 3 is completely determined by a single nondimensional parameter $\alpha^* = (\alpha/c)(T_e - T_c)$, which measures the strength of dynamic coupling relative to the thermodynamic forcing. For a fixed strength of dynamic coupling, α^* measures the capacity of the radiative feedbacks to trap heat. The values of T_e and c are given by

$$T_e \simeq T_0 + H_0\left(\frac{\partial E}{\partial T} - \frac{\partial G_a}{\partial T} - \frac{\partial C_l}{\partial T} - \frac{\partial C_s}{\partial T}\right)^{-1} \quad (4)$$

$$c = \frac{1}{C_p \rho h}\left(\frac{\partial E}{\partial T} - \frac{\partial G_a}{\partial T} - \frac{\partial C_l}{\partial T} - \frac{\partial C_s}{\partial T}\right) \quad (5)$$

where H_0 is the net heating of the coupled ocean-atmosphere evaluated at a reference temperature T_0, E is the surface emission, G_a is the clear-sky greenhouse effect, C_l is the greenhouse effect of clouds, C_s is the cloud shortwave forcing, and T = SST. Therefore, $\partial G_a/\partial T$, $\partial C_l/\partial T$, and $\partial C_s/\partial T$ are the radiative feedbacks of water vapor and clouds (3). In Eq. 5, ρ is the density of water, C_p is the specific heat, and h is the depth of the surface ocean. We obtained Eq. 4 by linearizing the net heating of the coupled ocean-atmosphere in a radiative-convective equilibrium. In deriving Eq. 5, we assumed that the atmosphere is always in thermal equilibrium with the underlying ocean. Equations 4 and 5 show that the more positive the radiative feedbacks of water vapor and clouds, the larger the T_e and the smaller the c, both of which lead to a larger α^*.

The coupled system contains two equilibrium states (Fig. 2). For $\alpha^* < 1$, the equilibrium is the radiative convective equilibrium, a warm stable state that has no ocean currents. For $\alpha^* > 1$, the radiative convective equilibrium becomes unstable, and a new state with ocean currents is switched on. The new state has a finite temperature difference between the east and the west and is colder than the radiative-convective equilibrium. Thus, Fig. 2 shows that in the presence of large positive feedbacks from water vapor or clouds, the coupled system is able to drift automatically from a state without ocean currents to a state with ocean currents. The ocean currents transport heat from the surface ocean to the subsurface ocean, counteracting the positive feedbacks from the atmosphere that tend to warm the surface ocean.

Figure 2 further shows that once the system is in the cold state with ocean currents, the larger the T_e, the larger the difference between T_e and T_1. This relation leads to an effective regulation on the temperature of the surface ocean. This regulatory effect may limit the temperature of the surface ocean to below 305 K even in the absence of cloud feedbacks (Fig. 3).

The replacement of the three-box ocean model with an ocean general circulation model (GCM) leads to similar results (9). Parameterizing the heat exchange with the atmosphere the same way as in the box model and coupling the east-west surface stress with the east-west SST differences, we again found that the ocean in the model has two equilibrium states: a warm state that has no wind-driven currents and a cold state that has wind-driven currents. The warm state became unstable when the coupling between the wind stress and the east-west SST differences was sufficiently strong (or equivalently when the net radiative feedback from water vapor and clouds was sufficiently positive): The ocean GCM exhibits the same feature as the three-box ocean model (Fig. 4).

The equation that determines the sensitivity of the SST in the western Pacific Ocean may be written as

$$\delta T \simeq H_w(T_0)\left(\frac{\partial F_o}{\partial T} + \frac{\partial E}{\partial T} - \frac{\partial G_a}{\partial T} + \frac{\partial F_{as}}{\partial T} - \frac{\partial C_l}{\partial T} - \frac{\partial F_{al}}{\partial T} - \frac{\partial C_s}{\partial T}\right)^{-1} \quad (6)$$

where δT is the SST deviation from a reference temperature T_0, H_w is the net heating of the coupled ocean-atmosphere column over the western Pacific region, and $H_w(T_0)$ is H_w evaluated at T_0. We obtained Eq. 6 by linearizing H_w about T_0. The parameters F_o and F_{as} are, respectively, the heat transports by ocean currents and atmospheric circulations; F_{al} is the

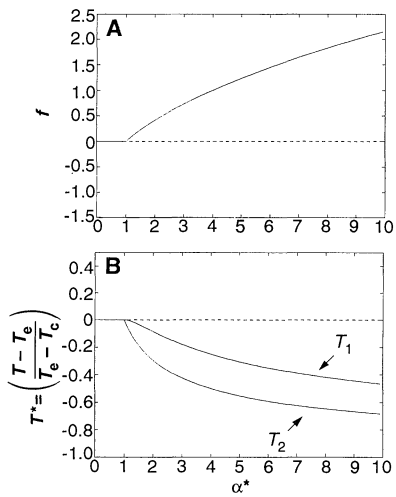

Fig. 2. Equilibrium solutions for the coupled model. (**A**) Strength for the ocean current. Plotted is $f = q/c$. The two equilibrium solutions are $f = 0$ and $f = \sqrt{\alpha^*} - 1$. The latter solution exists only when $\alpha^* > 1$. (**B**) Surface ocean temperatures. Plotted are $T_1^* = (T_1 - T_e)/(T_e - T_c)$ and $T_2^* = (T_2 - T_e)/(T_e - T_c)$. For $f = 0$, $T_1^* = T_2^* = 0$. For $f = \sqrt{\alpha^*} - 1$, $T_1^* = -1 + (2/\sqrt{\alpha^*}) - (1/\alpha^*)$, and $T_2^* = -1 + (1/\sqrt{\alpha^*})$. The dashed line indicates that the solution exists but is unstable.

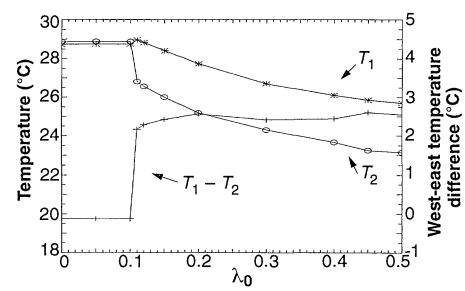

Fig. 4. The equilibrium SST in the western and eastern tropical Pacific oceans as a function of the coupling strength λ_0. The temperatures T_1 and T_2 are area-averaged SSTs for the western and eastern tropical Pacific, respectively, and λ_0 measures the sensitivity of wind stress to changes in SST gradients; λ_0 is proportional to α in Eq. 3, and varying λ_0 is equivalent to varying α^*. See (15) for details.

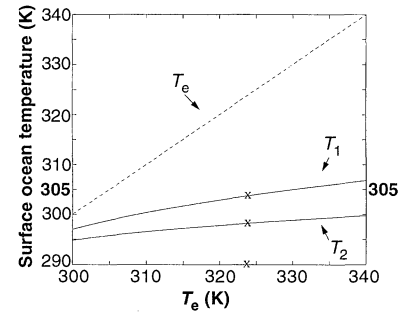

Fig. 3. The temperatures T_1 and T_2 as a function of T_e for $c = 1.5 \times 10^{-8}\ s^{-1}$, $\alpha = 1.0 \times 10^{-8}\ K^{-1}\ s^{-1}$, and T_c = 18°C. The value of c corresponds to a zero cloud feedback and was obtained from Eq. 5 with the use of the water vapor feedback from Sun and Oort (12) and h = 50 m. The observed annual mean values for the strength of the equatorial surface ocean current and SST gradients were used to estimate α. (A direct estimate of α may be obtained with use of the standard eddy-damping time scale in the atmospheric and oceanic boundary layer, which gives a similar value.) Although T_1 and T_2 increase with T_e, the rate of increase is so small that they are practically independent of T_e. As long as T_e does not exceed 329 K, T_1 will be effectively limited to less than 305 K. In the absence of cloud feedbacks, the maximum T_e is only about 324 K (14). The maximum T_e and the corresponding T_1 and T_2 are marked in the figure (×). The maximum values for T_1 and T_2 are not sensitive to the strength of water vapor feedback. The value of c may become larger (smaller) for a weaker (stronger) water vapor feedback, but T_e will become smaller (larger) (Eqs. 4 and 5).

heating due to the net moisture convergence. Equation 6 shows that it is the derivative of the oceanic transport with respect to SST, not the magnitude of the oceanic transport, that determines the sensitivity of the tropical SST. This fact was overlooked by Ramanathan and Collins (*10*). The equation also shows that the effectiveness of the feedback from ocean currents depends crucially on the nature of other feedbacks. Over the warm pool region, $\partial E/\partial T$ is largely canceled by $\partial G_a/\partial T$, and $\partial C_l/\partial T$ is largely balanced by $\partial F_{as}/\partial T$ (*3*). There may be further cancellations between $\partial C_s/\partial T$ and $-\partial F_{al}/\partial T$ because increased cloudiness over the warm pool region is likely accompanied by enhanced moisture convergence (*4*). The larger cancellation among atmospheric feedbacks makes the feedback from ocean currents crucially important. Moreover, all of the feedback terms in Eq. 6 depend strongly on the Walker circulation (*4, 5*) and therefore more fundamentally on the dynamic coupling between the atmosphere and ocean. It is the dynamic coupling that gives rise to the east-west SST gradients and the accompanying Walker circulation.

REFERENCES AND NOTES

1. T. J. Crowley and G. R. North, *Paleoclimatology* (Oxford Univ. Press, New York, 1991).
2. S. G. H. Philander, *El Niño, La Niño, and the Southern Oscillation* (Academic Press, New York, 1989).
3. V. Ramanathan and W. Collins, *Nature* **351**, 27 (1991).
4. R. Fu, A. D. Del Genio, W. B. Rossow, W. T. Liu, *ibid.* **358**, 394 (1992).
5. D. E. Waliser and N. E. Graham, *J. Geophys. Res.* **98**, 12881 (1993); J. M. Wallace, *Nature* **357**, 230 (1992); D. Hartmann and M. Michelsen, *J. Clim.* **6**, 2049 (1993); R. T. Pierrehumbert, *J. Atmos. Sci.* **52**, 1784 (1995).
6. R. S. Lindzen and S. Nigam, *J. Atmos. Sci.* **44**, 2418 (1987).
7. J. C. McWilliams and P. R. Gent, *ibid.* **35**, 963 (1978).
8. The long-term coldness of the equatorial subsurface ocean is maintained by the meridional branch of the wind-driven circulation, which moves heat to the extratropical ocean (*11*).
9. R. C. Pacanowski, K. W. Dixon, A. Rosati, "The GFDL Modular Ocean Model users guide," *GFDL Ocean Group Tech. Rep. 2* (1991).
10. $H_w = S_c + C_s + G_a + C_l - E - F_o - F_{as} + F_{al}$, where S_c is the clear-sky solar radiation. Ramanathan and Collins (*3*) dropped F_o from H_w before it was perturbed to obtain Eq. 6.
11. J. McCreary and P. Lu, *J. Phys. Oceanogr.* **24**, 466 (1994); Z. Liu, G. Philander, R. Pacanowski, *ibid.*, p. 2606.
12. D.-Z. Sun and A. H. Oort, *J. Clim.* **8**, 1974 (1995).
13. K. Bryan, *J. Phys. Oceanogr.* **14**, 666 (1984).
14. This estimate was obtained from Eq. 4. The upper limit for H_0 was taken as $S_c + G_a(T_0) - \sigma T_0^4$, where $S_c = 370$ W m^{-2} (clear-sky solar radiation), $G_a = 165$ W m^{-2}, σ is the Stefan-Boltzmann constant, and $T_0 = 300$ K. The same values for S_c, G_a, and T_0 were used by Ramanathan and Collins (*3*). The value for water vapor feedback was from Sun and Oort (*12*).
15. The ocean model domain spans 40° in longitude and 3000 m in depth from 2°S to 50°N, with a resolution of 2° in both latitude and longitude and 15 levels in the vertical. With no wind imposed on the ocean, we first spun up the ocean GCM for 1000 years for the surface layer and 5000 years for the bottom layer using an acceleration scheme given by Bryan (*13*). The heat exchange between the atmosphere and ocean had the same form as in the box model, with T_e varying with latitude following a cosine profile from 319 K at the equator to 263 K at 50°N. The thermal relaxation time scale $1/c$ was chosen as 200 days. The salinity field was held constant. The spin-up was to allow the thermohaline circulation to set up a basic temperature structure for the ocean. Except near the western boundary, distributions of SST in such a state were essentially zonally symmetric. A perturbation to the upper ocean was introduced by imposing a weak wind stress for a year. The surface wind was then coupled to the east-west SST differences in a way similar to that for the box model: $\tau_x = \lambda_0[\eta(y)](T_1 - T_2)$, where τ_x is the east-west wind stress, λ_0 is the coupling strength, and $\eta(y)$ is a specified function of latitude y that gives easterly wind in the tropics and westerly wind in the extratropics. The domains over which T_1 and T_2 were obtained spanned latitudes of 0° to 10°N and longitudes of, respectively, 0° to 15° and 25° to 40° of our 40° region. Thirteen experiments with different λ_0 were conducted. For small λ_0, no significant east-west SST gradients were developed, and the ocean returned to the basic state without wind. When λ_0 was sufficiently large, however, the ocean drifted quickly to a new state with significant east-west SST differences. No significant changes were found after the first two decades of integration, indicating that the heat transfer is mainly a balance between the radiative convective processes and the wind-driven circulations. In the GCM experiments, heat was gained in the tropics and lost in the extratropics, as in the observations. Plotted in Fig. 4 are values of T_1 and T_2 at the end of 50 years of integration. (A few experiments were extended to 1000 years of integration, and no significant differences from the corresponding 50 years of integration were found.)

16. We gratefully acknowledge helpful comments from F. Bryan, P. Gent, I. Held, J. Kiehl, R. Lindzen, J. McWilliams, K. Trenberth, J. Tribbia, P. Webster, and the reviewers. This work was supported by the National Science Foundation and the National Oceanic and Atmospheric Administration.

10 October 1995; accepted 1 March 1996

Fossil Evidence for a Late Cretaceous Origin of "Hoofed" Mammals

J. David Archibald

Seventeen of eighteen orders of living placental mammals are not known before 65 million years ago. The monophyly of each order is well established, but interrelations have been less certain. A superordinal grouping of up to seven extant orders plus a variety of extinct orders, all included within Ungulata ("hoofed" mammals), can be linked to Late Cretaceous mammals from the 85-million-year-old Bissekty Formation, Uzbekistan (and, less certainly, North America and Europe), thus pushing the origin of this major clade back by 20 million years. Ungulatomorphs are not closely related to primates, rodents, or rabbits.

Whether they include one (aardvarks) or 1750 (rodents) extant species, orders are the most inclusive groupings for which there is certainty of monophyly within Mammalia. The monophyly of superordinal taxa such as Ungulata has been much less certain (*1*). The mammalian division Ungulata is usually argued to include archaic ungulates ("Condylarthra") (*2*), South American native ungulates (*3*), Desmostylia, and Embrithopoda, and the extant Artiodactyla, Cetacea, Hyracoidea, Perissodactyla, Proboscidea, Sirenia, and questionably Tubulidentata, but it excludes the extinct Pantodonta, Tillodontia, and Dinocerata (*4*). None of these orders had been known from before the earliest Tertiary [65 million years ago (Ma)] except for questionable Late Cretaceous occurrences in North and South America (*5*). Fossils recovered from the 85-million-year-old Bissekty Formation, Uzbekistan (*6*), however, appear to have ungulate affinities (*7, 8*) on the basis of dental morphology that seems to mark the beginnings of herbivory in placental mammals. These fossils, plus possibly others from North America and Europe, comprise the family "Zhelestidae" (*9*). A review of the biostratigraphy of the Bissekty Formation (*10*) corroborates the ~85-million-year age estimate and also suggests that various of its named and unnamed mammalian species are best referred to "Zhelestidae." In this report, I present the results of a species-level phylogenetic analysis of better known, Late Cretaceous placental mammals, including the "zhelestids," plus Ungulata. Trends in increased herbivory among "zhelestids" compared to other Late Cretaceous placental mammals are also discussed.

The phylogenetic analysis (Fig. 1) of all species of better known Late Cretaceous placental mammals (Table 1) shows that "zhelestids" are monophyletic relative to other Late Cretaceous eutherians. The upper and lower dentitions of the mid-sized Asian "zhelestids" cannot at this time be matched; thus, the study was limited to the better known upper dentition. As shown in Fig. 1, the analysis includes Tertiary Ungulata represented by *Protungulatum* (or *Oxyprimus*) as an exemplar. Because some "zhelestids" have a more recent common ancestry with Ungulata than with other "zhelestids," "Zhelestidae" is paraphyletic (and thus the quotation marks). With Ungulata, however, "Zhelestidae" forms a clade

Department of Biology, San Diego State University, San Diego, CA 92182, USA.